Journal of the Geological Society, London, Vol. **166**, 2009, pp. 783–796. doi: 10.1144/0016-76492008-019.

Inclusion study in zircon from ultrahigh-pressure metamorphic rocks in the Kokchetav massif: an excellent tracer of metamorphic history

IKUO KATAYAMA[1]* & SHIGENORI MARUYAMA[2]

[1]*Department of Earth and Planetary Systems Science, Hiroshima University, Hiroshima 739-8526, Japan*

[2]*Department of Earth and Planetary Sciences, Tokyo Institute of Technology, Tokyo 152-8551, Japan*

**Corresponding author (e-mail: katayama@hiroshima-u.ac.jp)*

Abstract: Zircon is an excellent material to preserve the complex history of ultrahigh-pressure (UHP) metamorphic rocks, whereas mineralogical evidence of UHP conditions is mostly obliterated in matrix assemblages as a result of extensive retrograde overprinting during exhumation. Zircons from the Kokchetav UHP–HP massif contain numerous inclusions of graphite, quartz, garnet, omphacite, jadeite, phengite, phlogopite, rutile, albite, K-feldspar, amphibole, zoisite, kyanite, calcite, dolomite, apatite and monazite, as well as the diagnostic UHP minerals, such as microdiamond and coesite, which were identified by laser Raman spectroscopy. The internal structure of zircon displays a distinct zonation, which comprises an inherited core, a wide mantle and an outer rim, each with distinctive inclusion micro-assemblages. The low-pressure mineral inclusions, such as graphite, quartz and albite, are common in the inherited core and thin outer rim, whereas diamond, coesite and jadeite occupy the mantle domain. The zircon core and outer rim are of detrital and relatively low-grade metamorphic origin, whereas the mantle domain is of HP to UHP metamorphic origin. The mineral assemblages and chemistry of inclusions preserved in zircon have been used to constrain the metamorphic *P–T* path of the Kokchetav UHP–HP rocks, and indicate peak metamorphism at 60–80 kbar and 970–1100 °C followed by nearly isothermal decompression at 10 kbar and *c*. 800 °C. Sensitive high-resolution ion microprobe U–Pb spot analyses of the zoned zircon indicate four discrete ages of the Kokchetav metamorphic evolution: (1) a Middle Proterozoic protolith age; (2) 537 ± 9 Ma for UHP metamorphism; (3) 507 ± 8 Ma for the late-stage amphibolite-facies overprint; (4) 456–461 Ma for post-orogenic thermal events. This indicates that Middle Proterozoic supracrustal protoliths of the Kokchetav UHP–HP rocks were subducted to mantle depths in the Middle Cambrian, and exhumed to mid-crustal levels in the Late Cambrian. The zonal arrangement of inclusions and the presence of coesite and diamond without back reaction imply that aqueous fluids were low to absent within zircon, and that zircon is capable of retaining minerals of each metamorphic stage. We suggest that the study of inclusions in zircon is a powerful method to clarify the multiple stages and timing of metamorphic evolution of UHP–HP rocks, the evidence for which has been more or less obliterated in the host rock.

The discovery of *in situ* metamorphic microdiamonds in garnet biotite gneisses, dolomitic carbonates and garnet pyroxenites from the Kokchetav massif (Sobolev & Shatsky 1990) has greatly increased estimates of the maximum pressure attained by crustal metamorphic rocks in collisional orogenic belts. The tectonic and petrological implications for subduction of continental materials to depth in excess of 150 km has led to considerable interest in these unusual rocks and their metamorphic evolution (e.g. Liou *et al*. 1994; Coleman & Wang 1995; Harley & Carswell 1995). However, vestiges of ultrahigh-pressure (UHP) metamorphic mineral assemblages constitute only a minor component of these rocks (e.g. Liou *et al*. 1994; Coleman & Wang 1995; Harley & Carswell 1995), and have been mostly obliterated by extensive hydration and replaced by low-pressure mineral assemblages during a late amphibolite-facies overprint related to exhumation. Mineralogical evidence of the extreme conditions of UHP metamorphism is largely restricted to armoured inclusions within refractory minerals such as garnet or zircon. Harley & Carswell (1995) considered that this problem is related to access of fluids into the rocks undergoing metamorphism because of their catalytic role in promoting reactions (Rubie 1986; Austrheim 1998). Hence, zircon is considered to be the best container of UHP metamorphic minerals because of its stability over a wide *P–T* range, its mechanical resistance, and its ubiquitous occurrence as an accessory mineral in metamorphic rocks (Chopin & Sobolev 1995; Tabata *et al*. 1998). We have systematically investigated mineral inclusions preserved in zircon from various rocks in the Kokchetav massif to reveal primary mineral assemblages and metamorphic zonation in this area. The distribution of micro-inclusions in zircon shows a good correlation with the zircon zonal texture, and we dated such zircon by sensitive high-resolution ion microprobe (SHRIMP) U–Pb spot analysis to constrain the timing of discrete stages of metamorphic evolution. This paper summarizes our recent progress in understanding the metamorphic *P–T*–time path of the Kokchetav UHP–HP rocks, which was published previously (Katayama *et al*. 2000*a*,*b*, 2001), with some additional data. We conclude that the study of micro-inclusions preserved in zircon is a powerful tool to understand the complex metamorphic history of deeply subducted materials.

Geological outline of the Kokchetav UHP–HP massif

The Kokchetav massif is situated in the central domain of the composite Eurasian craton, and was formed during Cambrian collisional orogenic events (Dobretsov *et al*. 1995). This massif is composed of several Precambrian rock series, Cambro-Ordovician volcanic and sedimentary rocks, Devonian volcanic molasse, and Carboniferous–Triassic shallow-water and lacustrine sedi-

ments; these rocks were intruded by multi-stage granitoids (Dobretsov *et al*. 1995). The UHP–HP metamorphic part of the massif is a thin (1–2 km), more or less coherent, subhorizontal sheet, which is structurally overlain by a weakly metamorphosed unit (unit V), and underlain by the Daulet Suite (Kaneko *et al*. 2000). The UHP–HP massif is subdivided into four units based on gross lithological variations (Fig. 1). Unit I is composed of amphibolite and acidic gneiss, unit II is composed mainly of pelitic–psammitic gneiss with locally abundant eclogite boudins and marble, unit III is composed of alternating orthogneiss and amphibolite with rare eclogite lenses, and unit IV is composed of quartz schist and siliceous schist (Kaneko *et al*. 2000). Eclogites occur as lenticular masses within diamond-bearing gneiss and marble, and yield maximum P–T conditions of $P > 60$ kbar and $T > 1000$ °C based on the K_2O-in-augite geobarometer and Grt–Cpx geothermometer (Okamoto *et al*. 2000). Metamorphic diamonds have been identified in pelitic gneisses, marbles and garnet pyroxenites from the Kumdykol region (Sobolev & Shatsky 1990; Zhang *et al*. 1997; Katayama *et al*. 2000*a*; Ogasawara *et al*. 2000). Coesite also occurs widely in eclogite, pelitic gneiss and whiteschist as inclusions in zircon and garnet from the Kumdykol, Barchikol and Kulet regions (Shatsky *et al*. 1995; Korsakov *et al*. 1998; Katayama *et al*. 2000*a*; Parkinson 2000). Other mineralogical and textural indicators of UHP metamorphism, such as exsolved silica rods in omphacite, K-rich pyroxene, Si-rich phengite, and aluminous titanite, are also present in the Kokchetav UHP–HP part of the massif (Shatsky *et al*. 1995; Zhang *et al*. 1997; Katayama *et al*. 2000*b*; Ogasawara *et al*. 2000, 2002; Okamoto *et al*. 2000).

Previous geochronological studies have reported the timing of the Kokchetav UHP–HP metamorphism using various methods. A mean U–Pb zircon age from diamond-bearing gneisses of 530 ± 7 Ma was interpreted to represent the peak-metamorphic age (Claoue-Long *et al*. 1991). Zircon xenocrysts as old as 2000 Ma have also been reported, interpreted as representing an Early Proterozoic protolith age (Claoue-Long *et al*. 1991). Clinopyroxene and garnet from eclogite were dated at 533 ± 20 Ma by the Sm–Nd isochron method (Jagoutz *et al*. 1990). Muscovite and biotite separated from diamond-bearing gneiss yielded ^{40}Ar–^{39}Ar ages of 517 ± 5 Ma and 516 ± 5 Ma, respectively, which have been interpreted as a cooling age (Shatsky *et al*. 1999).

Analytical methods

Zircons were extracted using a mineral separation system at Tokyo Institute of Technology. After crushing and sieving of a *c*. 200 g sample, magnetic and heavy liquid separations were performed. The separated zircon grains (50–300 grains for each sample) were then mounted and polished in 25 mm epoxy discs. Mineral inclusions in zircons were identified by laser Raman micro-spectroscopy (using a JASCO NRS-2000C system) with the 514.5 nm line of an Ar-ion laser in the same laboratory. Chemical compositions of inclusions were analysed by electron microprobe analysis (using a JEOL JXA 8800 system) with a 15 kV accelerating voltage and 12 nA beam current. The internal zoning pattern of the crystal sections was observed by cathodoluminescence (CL) and secondary electron microscopy.

The zircon grains mounted on epoxy discs were then used for U–Th–Pb dating using a SHRIMP II at Hiroshima University. Instrumental conditions and measurement procedures have been described by Sano *et al*. (2000). The spot size of the ion beam was *c*. 20 μm; seven scans through the critical mass range were made for data collection. The $^{206}Pb/^{238}U$ ratio in the samples was calibrated by using an empirical relationship of Claoue-Long *et al*. (1995) and corrected by using reference zircon SL13 from Sri Lanka (572 Ma). The common-Pb correction used the $^{206}Pb/^{204}Pb$ ratio and assumed a two-stage evolution model (Stacey & Kramers 1975). Trace element analysis of zircons was performed by laser-ablation inductively coupled plasma mass spectrometry (LA-ICP-MS) at Tokyo Institute of Technology (Iizuka & Hirata 2004). Ablation was carried out with a pulsed 193 nm Ar excimer laser with 140 mJ energy at a repetition rate of 5 Hz and pit size of 20 μm. A helium stream was used to transport the sample effectively and reduce deposition at the ablation site (Eggins *et al*. 1998).

Primary assemblages of UHP conditions

Mineral inclusions in zircon from the Kokchetav UHP–HP rocks

We analysed a total of *c*. 12 000 zircon grains separated from 246 representative rock samples from each metamorphic zone of the Kokchetav UHP–HP massif, including para- and orthogneisses or schists, eclogites, marbles and quartz schist.

Abundant microdiamond inclusions in zircon (Fig. 2) were identified in pelitic gneisses and dolomitic marbles from the Kumdykol region, which is located in the central portion of the massif. The diamond-bearing zircons are usually rounded and colourless, and are 100–150 μm in size. In the host rocks, primary minerals were mostly replaced by amphibolite-facies mineral assemblages such as chlorite, amphibole and plagioclase.

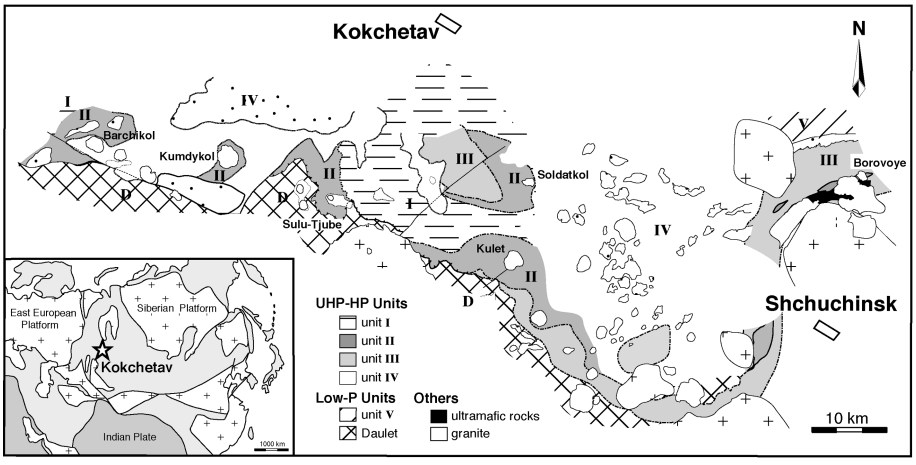

Fig. 1. Geological map of the Kokchetav UHP–HP massif (after Kaneko *et al*. 2000).

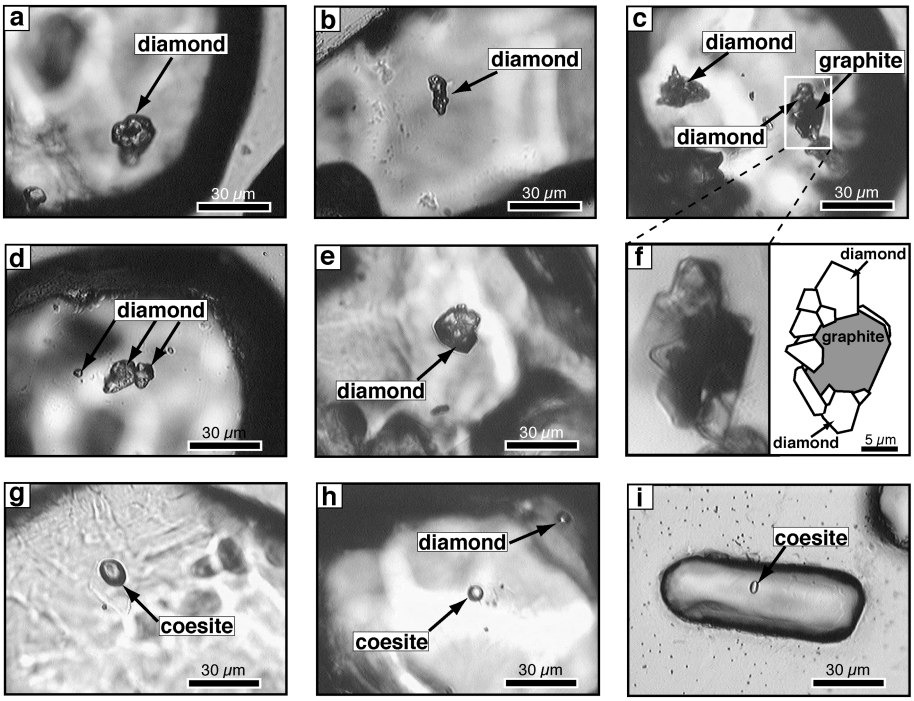

Fig. 2. Photomicrographs (plane-polarized light) showing diamond inclusions (**a**–**f**) and coesite inclusions (**g**–**i**) in zircon from the Kokchetav UHP metamorphic rocks. In (**f**) sketch of graphite and diamond aggregates in zircon is also shown.

Diamond inclusions in zircon were confirmed by the characteristic Raman peak at 1333 ± 2 cm^{-1} (Fig. 3a). Morphological forms comprise both octahedral and polycrystalline aggregates, *c*. 10 μm in diameter. Other UHP–HP inclusions such as coesite, jadeite and garnet coexist with diamond inclusions in zircon (Fig. 2). In addition, low-*P* minerals, including graphite, quartz and plagioclase, were also recognized as inclusions in zircon separated from the same sample. Graphite occurs as intergrowths with microdiamonds that display a botryoidal habit and clearly grew at the expense of graphite (Fig. 2f), whereas diamonds found in garnet are commonly surrounded by graphite along cracks, as a result of ingress of fluids. Coarse-grained graphite occurs in the zircon core, although most diamonds are distributed within the mantle domain, and, occasionally, small amounts of graphite also occur in the zircon outer rim. The inclusion micro-assemblages show a good correlation with the host zircon zonal texture seen in back-scattered electron (BSE) and CL images as described below.

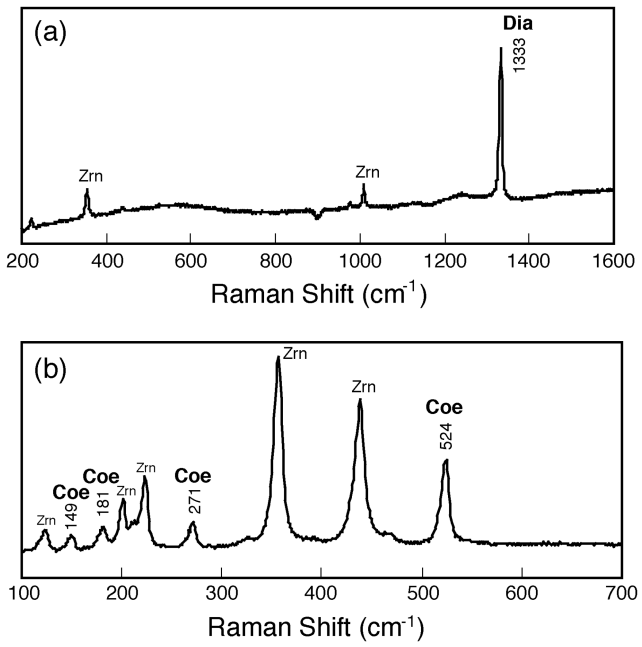

Fig. 3. Representative Raman spectra of (**a**) diamond and (**b**) coesite. Inclusion spectra always contain host zircon peaks at 359–362 cm^{-1}, 440–445 cm^{-1} and 1010–1013 cm^{-1}.

Coesite inclusions are identified in zircon separated from diamond-bearing pelitic gneisses, marbles, and eclogites from Kumdykol, and quartz schist from Barchikol. Zircons from eclogites are subhedral to anhedral, and generally homogeneous in BSE images. Grain sizes were smaller (50–80 μm) than those in diamond-bearing gneisses. Most coesite inclusions in zircon are ovoid and up to 10 μm in diameter (Fig. 2), and are identified by the characteristic Raman spectrum at 523 ± 2 cm^{-1} and weaker peaks at 271 ± 1 cm^{-1}, 181 ± 2 cm^{-1} and 149 ± 1 cm^{-1} (Fig. 3b). Diamond-bearing dolomitic marble also contains coesite as inclusions in zircon, whereas SiO_2 phases were absent in matrix assemblages. This suggests that silica phases were completely consumed by the prograde reaction dolomite + SiO_2 = diopside + CO_2, whereas zircon preserved relict coesite as inclusions.

Zircons separated from the other regions contain relatively low-*P* mineral inclusions, and show different characteristics from the UHP phase-bearing zircons; they are euhedral, elongated and prismatic, and usually exhibit oscillatory zonal fabrics. Apatite and quartz inclusions are ubiquitous in these zircons, and rutile and phengite inclusions are commonly observed (Table 1).

Inclusion assemblages preserved in zircon and metamorphic facies

Primary UHP metamorphic minerals are more or less obliterated during pervasive retrograde metamorphism, especially in country gneisses, as a result of ingress of fluids into the host rocks. The fragmental, incomplete evidence of UHP metamorphism provided by matrix assemblages greatly obscures characterization of

Table 1. *Representative mineral inclusion assemblages in zircon from the Kokchetav UHP–HP massif*

Locality	Sample number	Rock type	Dia	Grp	Coe	Qtz	Grt	Phe	Phl	Rt	Ab	Kfs	Amp	Cpx	Zo	Ky	Cal	Dol	Ap	Mz
Barchikol	F464	Pelitic gneiss				+	+	+		+										
Barchikol	F466	Pelitic gneiss		+		+	+	+		+	+									
Barchikol	F469	Amphibolite				+	+			+		+	+	+						
Barchikol	H318	Orthogneiss				+		+	+		+	+							+	+
Barchikol	K361	Quartzite			+	+							+	+			+	+		
Barchikol	K364	Eclogite				+	+			+		+		+	+				+	
Barchikol	Y410	Quartzite		+		+		+									+		+	
Kumdykol	A8	Pelitic gneiss	+	+	+	+	+			+				+					+	
Kumdykol	A12	Pelitic gneiss	+	+	+	+		+								+				
Kumdykol	A28	Pelitic gneiss		+		+	+	+		+	+									
Kumdykol	A30	Pelitic gneiss		+		+	+	+		+									+	
Kumdykol	A21	Eclogite			+	+	+			+	+		+	+					+	
Kumdykol	A60	Eclogite			+	+	+			+				+					+	
Kumdykol	H2	Pelitic gneiss	+		+		+										+			
Kumdykol	H5	Pelitic gneiss	+	+													+			
Kumdykol	K18	Pelitic gneiss		+		+		+				+							+	
Kumdykol	K183	Eclogite					+			+	+	+	+	+	+				+	
Kumdykol	N21	Metacarbonate	+	+	+		+						+	+			+	+	+	
Kumdykol	N57	Eclogite				+	+			+			+	+						
Kumdykol	XX7	Orthogneiss		+		+		+											+	
Chaglinka	K145	Pelitic gneiss		+		+	+	+											+	
Chaglinka	M121	Pelitic gneiss		+		+		+		+									+	
Chaglinka	T63	Pelitic gneiss				+		+		+										
Kulet	F256	Pelitic gneiss		+		+		+												
Kulet	F265	Pelitic gneiss				+		+		+		+							+	
Kulet	T264	Pelitic gneiss		+		+		+											+	
Sulu-Tjube	F44	Pelitic gneiss				+		+	+			+							+	
Sulu-Tjube	N81	Pelitic schist				+						+							+	
Soldatkol	F375	Quartz schist		+		+													+	+
Unit I	A157	Pelitic schist				+														
Unit III	Y276	Orthogneiss		+		+		+											+	

Dia, diamond; Grp, graphite; Coe, coesite; Qtz, quartz; Phe, phengite; Phl, phlogopite; Rt, rutile; Ab, albite; Kfs, K-feldspar; Amp, amphibole; Cpx, clinopyroxene; Zo, zoisite; Ky, kyanite; Cal, calcite; Dol, dolomite; Ap, apatite; Mz, monazite.

metamorphic zonation in UHP metamorphic terranes. Attempts to constrain the metamorphic zonation in the Kokchetav massif were made on the basis of mineralogical assemblages in metabasites (Masago 2000; Ota *et al*. 2000). The metabasites were divided into three metamorphic zones: (1) epidote–amphibolite facies; (2) amphibolite facies; (3) eclogite facies. However, thus far, the matrix mineral assemblages in metabasites cannot be used to further subdivide eclogite-facies rocks because of the lack of UHP minerals in matrix assemblages as a result of the extensive overprinting. Our results on the zircon-hosted inclusion distribution in this massif can be used to further subdivide the eclogite-facies rocks, including both metabasites and country gneisses, into diamond-eclogite, coesite-eclogite, and quartz-eclogite zones, whereas mineral assemblages in the matrix contain little evidence of such UHP assemblages (Fig. 4). Although coesites were reported in garnet from the Kulet region (Parkinson 2000), the lack of UHP evidence in zircon from this region could be due to low Zr contents in the bulk rocks and the absence of further zircon growth in these rocks. However, zircon is generally ubiquitous in metamorphic rocks, and can protect primary UHP minerals from late-stage overprinting. The metamorphic facies of UHP rocks can therefore be classified not only from matrix mineral assemblages but also from mineral inclusions in zircon. Such inclusions in zircon have now been widely reported from other UHP metamorphic terranes including the Dora–Maira massif of the western Alps (Schertl & Schreyer 1996), the Western Gneiss Region in Norway (Carswell *et al*. 2001), the Erzgebirge in Germany (Massonne 2001), the Dabie Mountains (Tabata *et al*. 1998; Liu *et al*. 2001) and Sulu region (Ye *et al*. 2000; Liu *et al*. 2001, 2002, 2006), north Qaidam in NW China (Song *et al*. 2001), Sulawesi in Indonesia (Parkinson & Katayama 1999), the Kaghan valley in the Pakistan Himalaya (Kaneko *et al*. 2003) and SE Brazil (Parkinson *et al*. 2001). These studies reveal that, in addition to the UHP eclogites, the surrounding country gneiss has also experienced the UHP metamorphism during the continental collision, and the whole package of supracrustal rocks was once subducted to depths greater than 120 km.

Mineral compositions of inclusions in zircon

Clinopyroxenes in both eclogite and marble exhibit an exsolution texture of quartz and phengite (Fig. 5a and b). Other exsolution textures are also commonly observed in UHP metamorphic rocks, including ilmenite rods in olivine and clinopyroxene, magnetite plates or rods in olivine and clinohumite, monazite lamellae in apatite, and clinopyroxene needles in garnet (see compilation by Liou *et al*. 1998). Such exsolution textures are believed to form during the decompression stage (Liou *et al*. 1998); however, the mechanism of their production is not clear. Mineral inclusions preserved in zircon can preserve pre-exsolved chemical compositions and provide constraints on the exsolution mechanism of the UHP phases.

Clinopyroxene

Abundant quartz rods occur in matrix omphacite of eclogite from Kumdykol (Fig. 5a), whereas zircon-hosted omphacite inclusions have no exsolution lamellae (Fig. 5c and d). To assess the precursor composition before exsolution, we analysed omphacite inclusions trapped in zircon and compared these compositions with the matrix omphacites. Most analyses of clinopyroxene inclusions indicate nearly sufficient silica to occupy the tetrahedral site, so that there is relatively little ^{IV}Al; the excess Al

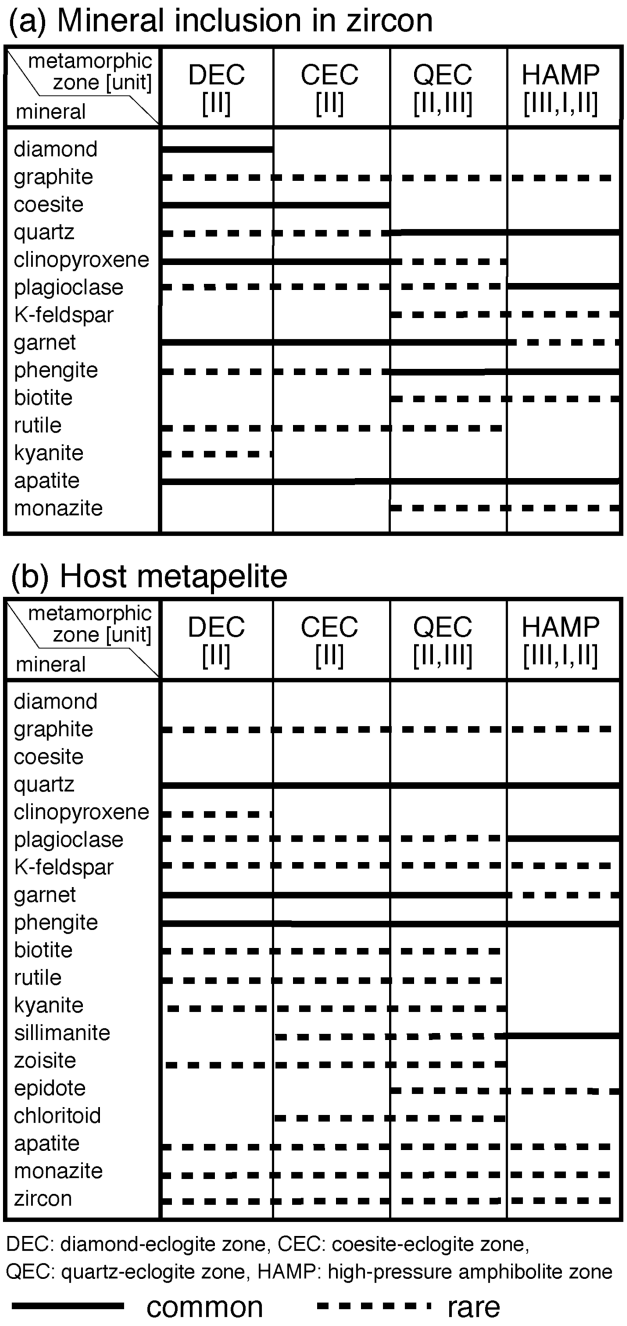

Fig. 4. (**a**) Inclusions in zircon from metapelites. (**b**) Host minerals in metapelites. Metamorphic zones and units are modified after Ota *et al*. (2000). Modified after Katayama *et al*. (2000*a*).

cannot be ascribed to the Ca-Tschermak molecule. The calculated cations indicate that a deficiency is maintained only by a significant portion of M-site vacancies. The stoichiometry of these pyroxenes can be reconciled best by consideration of the end-member Ca-Eskola component ($Ca_{0.5}\square_{0.5}AlSi_2O_6$, where $\square$ is a vacancy on the M_2 site). We therefore assumed eight pyroxene end-members: Ca-Eskola (CaEs), Ca-Tschermak (CaTs), jadeite (Jd), acmite (Acm), augite (Aug; diopside + hedenbergite), orthopyroxene (Opx; enstatite + ferrosilite), $Na(Mg,Fe)_{0.5}Ti_{0.5}Si_2O_6$ and $KAlSi_2O_6$. The end-member calculations were based on the method of Smyth (1980), with several modifications (for details see Katayama *et al*. 2000*b*).

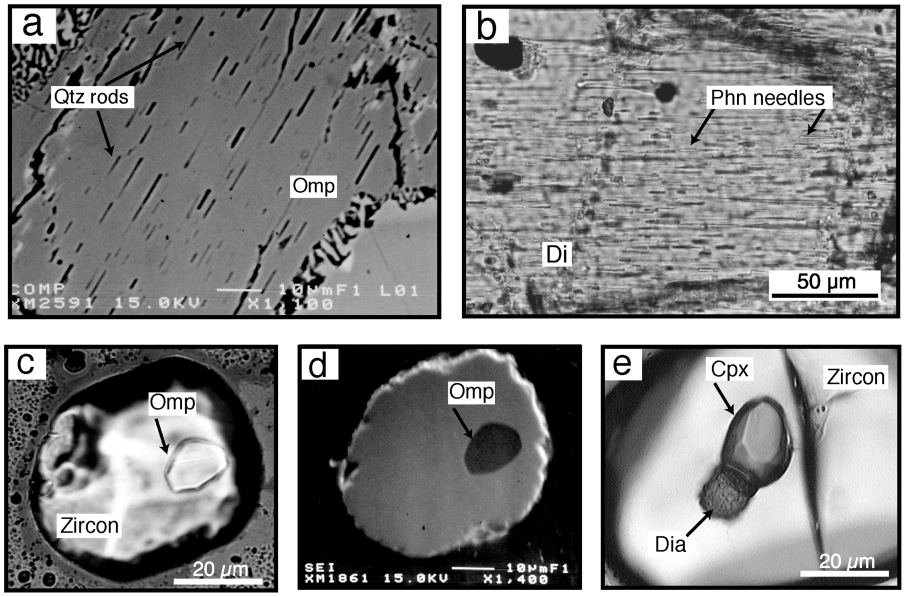

Fig. 5. Photomicrographs of matrix and inclusion minerals of the Kokchetav UHP rocks. (**a**) Omphacite from eclogite contains abundant quartz rods. (**b**) Diopside from diamond-bearing marble contains exsolved lamellae of phengite. (**c**, **d**) Omphacite inclusion in zircon from eclogite. Quartz rods are absent in the inclusion. (**e**) Diopside inclusion in zircon from marble, which is in contact with microdiamond inclusion.

Omphacite inclusions in zircon have significant amounts (up to 9.6 mol%) of the Ca-Eskola component, in contrast to the small amounts (1.3 mol%, on average) in the matrix omphacite. We calculated the original composition of matrix omphacite based on the quartz exsolution volume. The results indicate 6.6 mol% Ca-Eskola component in the original omphacite, which agrees with the inclusion composition in zircon. Figure 6 shows omphacite compositions plotted on an Augite–Jadeite–Ca-Eskola ternary diagram. Zircon-hosted omphacite tends to have higher Ca-Eskola component than matrix omphacite. The significant differences in the Ca-Eskola component between inclusion and matrix omphacite indicate that the quartz exsolution in matrix omphacite could be produced by a breakdown of this component. We therefore suggest that the Ca-Eskola component, which occurs at peak-metamorphic conditions, broke down by the reaction

$$2Ca_{0.5}\square_{0.5}AlSi_2O_6 = CaAl_2SiO_6 + 3SiO_2 \qquad (1)$$

resulting in the exsolution of quartz rods in matrix omphacite. The vacancy-containing Ca-Eskola clinopyroxene is reported to be sensitive to pressure and highly unstable at lower pressures (Mao 1971; Smyth 1980). Recent experimental studies found that, in addition to pressure, the Ca-Eskola component is also sensitive to temperature and bulk composition (Konzett *et al*. 2008).

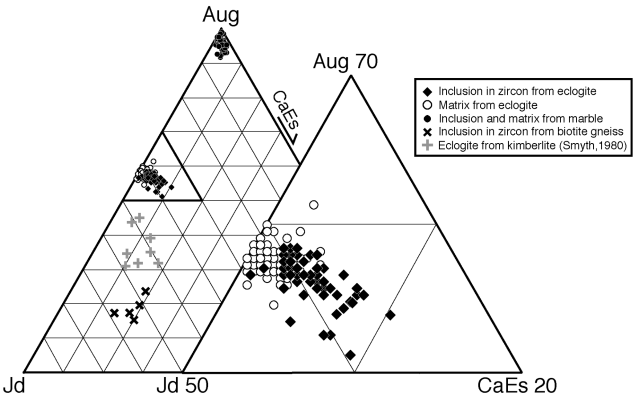

Fig. 6. Clinopyroxene compositions plotted on Augite–Jadeite–Ca-Eskola (Aug–Jd–CaEs) diagram (modified after Katayama *et al*. 2000*b*).

Rare jadeitic clinopyroxene inclusions were identified in zircon from the diamond-bearing biotite gneiss, whereas such clinopyroxenes are absent in the matrix phase. The jadeite inclusions also contain high Ca-Eskola component (13.4–18.6 mol%, Fig. 6). The higher Ca-Eskola component compared with those for eclogite may result from a high-Al bulk composition.

Diopside in a diamond-bearing dolomitic marble contains abundant exsolved lamellae, which are a few micrometres in diameter and *c*. 10 μm in length (Fig. 5b). It was difficult to obtain an accurate composition of the exsolution lamellae; however, elemental mapping shows Al and K concentrations in the lamellae, and laser Raman spectroscopy exhibits typical spectra of phengite with 260 cm^{-1} and 702 cm^{-1} peaks. The exsolution textures are, however, absent in the inclusion in zircon (Fig. 5e), and inclusions contain significant high K_2O and Ca-Eskola components, up to 0.56 wt% and 3.5 mol%, respectively, although matrix diopside has much lower contents of K_2O (0.14 wt%) and the CaEs component (2.1 mol%). Recalculated composition of matrix diopside involving 2.16 wt% phengite lamellae indicates 0.4 wt% K_2O and 2.7 mol% Ca-Eskola component for the original diopside, which is mostly consistent with compositions of the diopside inclusions in zircon. These suggest that phengite exsolution in diopside was produced by the reaction

$$\begin{aligned} &6\ KAlSi_2O_6 + 4\ Ca_{0.50.5}AlSi_2O_6 + 3\ (Mg,\ Fe)_2Si_2O_6 \\ &\quad + CaAl_2SiO_6 + 6\ H_2O \\ &\quad = 3\ Ca(Mg,\ Fe)Si_2O_6 + 6\ K(Mg,\ Fe)_{0.5}Al_2Si_{3.5}O_{10}(OH)_2 \\ &6\ \text{K-Jd} + 4\ \text{CaEs} + 3\ \text{Opx} + \text{CaTs} + 6\ \text{water} = 3\ \text{Aug} + 6\ \text{Phn}. \end{aligned} \qquad (2)$$

During decompression, K-jadeite and Ca-Eskola components became unstable at low pressures and temperatures, and reaction (2) was promoted, resulting in the exsolution of phengite needles in matrix clinopyroxene. The phengite exsolution in diopside

suggests that water included in phengite may have been initially incorporated within the precursor clinopyroxene at high pressures. According to the volume of phengite exsolution (2.6 vol.%), the precursor diopside contains *c*. 1000 ppm H_2O. Infrared and secondary ionization mass spectrometry (SIMS) analyses reveal high water concentrations in clinopyroxene from eclogites, up to 1500 ppm H_2O (Katayama & Nakashima 2003; Katayama *et al*. 2006).

Garnet

Garnet inclusions in zircon from the coesite-bearing eclogite are rare compared with omphacite inclusions. The chemical composition of garnets from both inclusions and matrix is plotted on the (Alm + Sps)–Prp–Grs ternary diagram (Fig. 7). Matrix garnets have almost homogeneous composition, slightly zoned with decreasing pyrope content from core to rim. On the other hand, garnet inclusions show a wide compositional variation: four crystals are Alm-rich (47–53%) and contain considerable spessartine (0.9–1.2%) component whereas the other grains are consistent with matrix garnet. Garnets contain detectable Na_2O (up to 0.15 wt%), which is consistent with previous studies in this region (Shatsky *et al*. 1995; Zhang *et al*. 1997; Okamoto *et al*. 2000). The high sodium content in garnet coexisting with a Na-bearing mineral is considered to be one of the important indicators of UHP metamorphism, as well as high K_2O content in clinopyroxene.

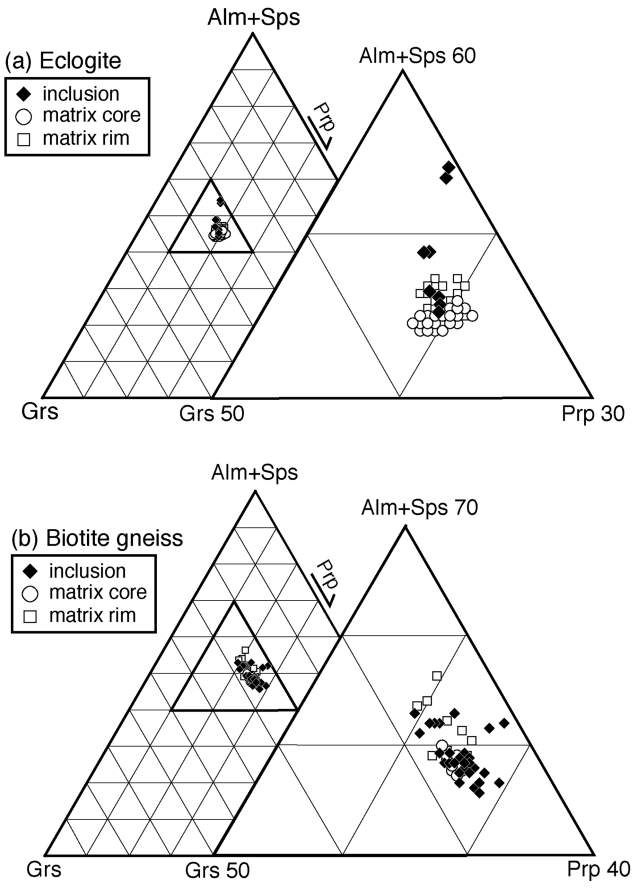

Fig. 7. Garnet compositions of inclusion and matrix plotted on ternary diagram of (Almandine + Spessartine)–Grossular–Pyrope. (**a**) Coesite-bearing eclogite; (**b**) diamond-bearing biotite gneiss.

Abundant garnet inclusions were identified in zircon from the diamond-bearing pelitic gneiss. Garnet inclusions are clear single crystals and are *c*. 10 μm in diameter, whereas matrix garnets are mostly fractured and replaced by secondary chlorite and biotite. Matrix garnet exhibits significant retrograde zonation with decreasing Prp contents from homogeneous core (24–26%) to rim (19–25%). Garnet inclusions show a relatively wide compositional range, extending toward the pyrope end-member. The maximum Prp content in garnet inclusions (29 mol%) is slightly higher than those in the matrix (26 mol%). Garnet in the diamond-bearing gneiss also contains significant amounts of sodium, up to 0.19 wt% Na_2O.

Rare garnet inclusions were identified in zircon from the diamond-bearing marble. They coexist with diamond inclusions in same zircon grain, and have high Grs (44%) and Prp (33%) components, whereas garnet is absent in matrix assemblage. Although garnets from other lithologies in Kumdykol have relatively high Na_2O contents, the sodium content is negligible in garnet from the diamond-bearing marble.

Micas

Phengite inclusions in zircon show higher Si content than those in matrix phengite from pelitic gneisses (up to 3.57 per 11 oxygens, Fig. 8), whereas the Fe/(Fe + Mg) ratio of inclusion and matrix phengites is limited in each sample. Phengite inclusions in the diamond-bearing marble have high Si contents (up to 3.53 p.f.u.) with a very low Fe/(Fe + Mg) ratio of 0.06, although phengite is absent in zircon separated from the diamond-bearing gneiss and the coesite-bearing eclogite. Phlogopite inclusions coexisting with microdiamond in zircon from marble have a higher Si content, 2.99–3.00 per 11 oxygens, and slightly higher Fe/(Fe + Mg) ratio of 0.11 than those of matrix phlogopite (Si 2.28–2.92 and Fe/(Fe + Mg) ratio 0.08–0.10). The Al/(Al + Si) ratio of inclusion phlogopite is higher than that of matrix.

Zircon geochronology assisted by inclusion micro-assemblages

The Kokchetav UHP–HP rocks have experienced a long and complex metamorphic evolution over a very wide range of *P*–*T* conditions. Radiometric age dating is a key to understanding the complex metamorphic history of these rocks. SHRIMP dating of discrete domains within zircon crystals, allied with CL image analysis, has contributed greatly to recent progress in dating metamorphic rocks (e.g. Gebauer *et al*. 1997; Liati & Gebauer 1999; Rubatto *et al*. 1999). Discrete zoned domains in zircon may reflect not only the peak-metamorphic stage, but also progressive and retrogressive stages of their metamorphic evolution. This can be clarified by identification of mineral inclusion micro-assemblages within each zircon domain.

Internal structure of zircon associated with inclusions

Zircons from the diamond-bearing gneisses are usually rounded, colourless and 100–200 μm in diameter. The CL and BSE investigations reveal internal structures of zircons, mainly consisting of core and rim domains; cores of low luminescence in CL image are surrounded by relatively bright luminescent rims (Fig. 9a and b). Complex zoned metamict cores rarely survive, and have relatively small domains of a bright luminescence in CL (Fig. 9a); they are interpreted as inherited domains. Zircons contain abundant microdiamond inclusions, and other inclusions

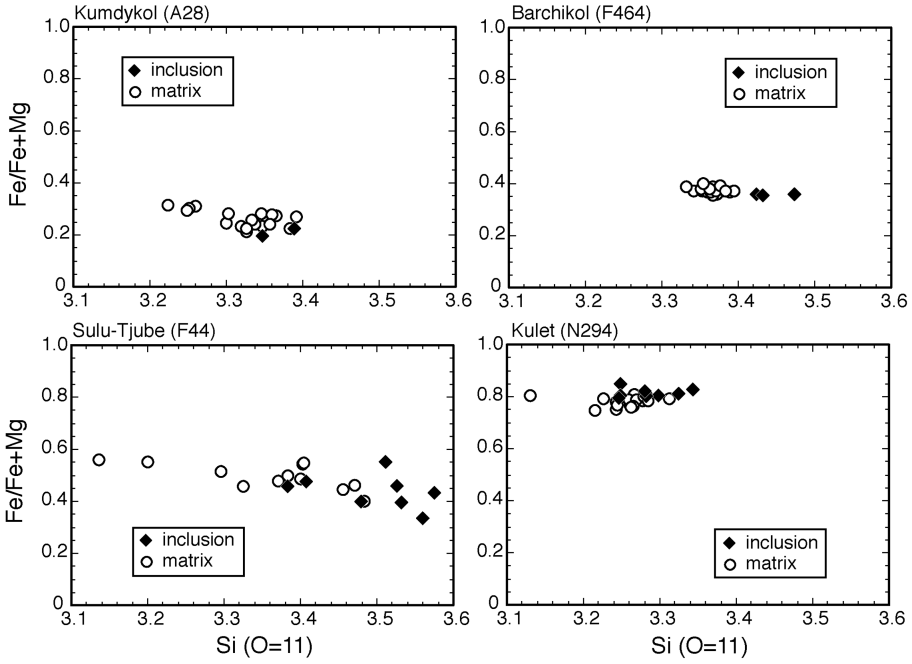

Fig. 8. Composition of analysed inclusion and matrix phengites from pelitic gneisses. Inclusions show higher Si content than the matrix phengites, whereas Fe/(Fe + Mg) ratios of the inclusion and matrix phengites are relatively limited in the samples.

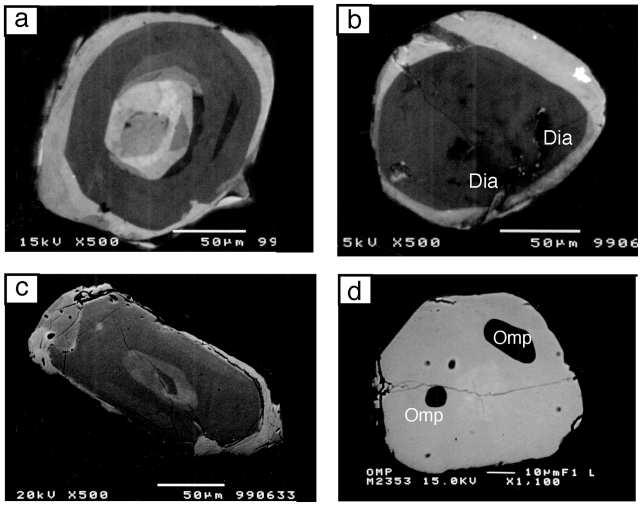

Fig. 9. CL images of zircons from diamond-bearing gneiss (**a**, **b**) and BSE images of zircons from low-grade schist (**c**) and from eclogite (**d**). Zircon from eclogite has no zonal texture and contains numerous inclusions including omphacite, garnet and coesite, whereas zircon from gneiss and schist shows clear zonal texture with distinct inclusion micro-assemblages.

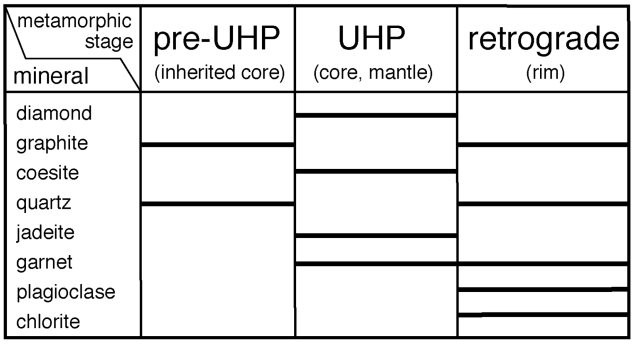

Fig. 10. Mineral inclusion assemblages in the various zircon domains of diamond-bearing gneisses (after Katayama *et al*. 2001).

include coesite, garnet, jadeitic pyroxene, rutile, phengite, kyanite, amphibole, plagioclase, chlorite, apatite, graphite and quartz (Table 1). Mineral inclusions are generally correlated with specific domains of zoned zircon. The core to mantle domains contain diamond, coesite and jadeite inclusions, whereas graphite, quartz, plagioclase and chlorite inclusions occur in the outer rims, and most inherited cores are inclusion-free or contain low-*P* minerals such as graphite and quartz (Fig. 10).

A low-grade pelitic schist from the Sulu-Tjube region contains euhedral and elongated zircons of *c*. 100 μm long axis length. The zircon morphology is very different from that in the diamond-bearing gneisses. In BSE and CL images, zircons consist of small cores, widely spaced euhedral oscillatory domains as typically observed for crystal growth from a melt, and thin outer unzoned rims with BSE bright luminescence (Fig. 9c). The inner boundary of oscillatory domains and rims is irregular, and the magmatic core is corroded by the homogeneous rims. These zircons contain quartz, muscovite, K-feldspar, chlorite, graphite and apatite as inclusions.

Eclogite contains abundant anhedral zircons of 50–70 μm diameter, which are apparently smaller than those of the pelitic gneisses. Zircon separated from eclogite contains the UHP phases such as coesite, K-rich omphacite and Na-rich garnet, and composite inclusions of garnet and albite (Okamoto *et al*. 2006). CL imaging reveals that most zircons are homogeneous without a magmatic core (Fig. 9d).

Zircon SHRIMP U–Pb dating

U–Pb isotopic data for the diamond-bearing zircon domains are mostly concordant (Fig. 11), and yield apparent $^{206}Pb/^{238}U$ ages ranging from 554 to 493 Ma (Table 2). Because they contain UHP mineral inclusions, such as diamond and coesite, these zircons clearly have grown under UHP conditions. The zircon outer rims generally exhibit younger ages than those of diamond-

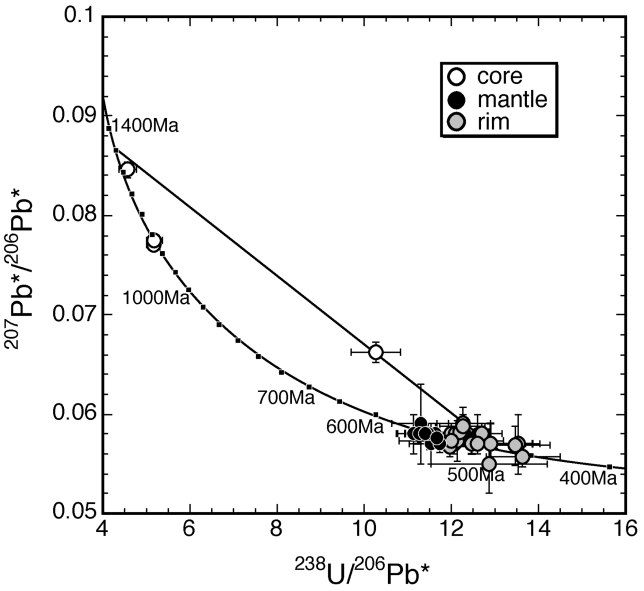

Fig. 11. Tera–Wasserburg diagram of SHRIMP analyses of the various zircon domains of the diamond-bearing gneisses and low-grade schist (modified after Katayama *et al*. 2001).

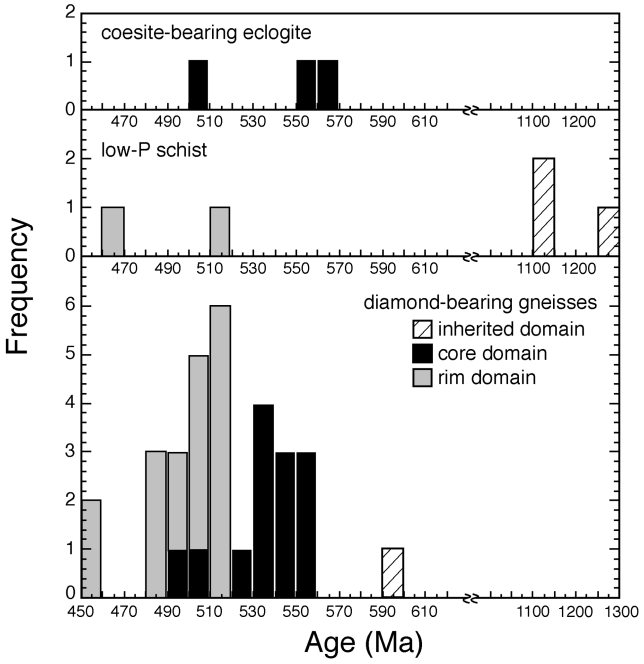

Fig. 12. Histogram of apparent $^{206}Pb/^{238}U$ age of the zircon domains of each lithology. The different zircon domains show apparently different ages (modified after Katayama *et al*. 2001).

bearing cores, ranging from 456 to 517 Ma (Fig. 11). The considerable difference in the apparent ages occurs even in single zircon grains. The inherited core yields a discordant age (Fig. 11), indicating that it has been affected by one or more Pb-loss events. Assuming that Pb loss from the core had occurred at the time of the latest metamorphism (*c*. 500 Ma), the upper intercepts of presumed mixing lines (discordias) indicate that the core had grown or metamorphosed in the Middle Proterozoic (*c*. 1300–1400 Ma). Zircons from low-grade schist yield $^{206}Pb/^{238}U$ ages of 1280–1140 Ma in the core and mantle domains, and apparently younger ages of 461–516 Ma in the outer rim (Fig. 12). The homogeneous zircons from the coesite-bearing eclogite are mostly concordant, and yield $^{206}Pb/^{238}U$ ages ranging from 569 to 506 Ma (Fig. 12). The large age variety and uncertainty may result from extremely low U concentration (42–66 ppm) in these zircon grains, whereas coesite and high Ca-Eskola omphacite inclusions clearly indicate that these zircons have grown at the UHP stages.

Zircon REE abundances

The REE pattern and abundance of zircon are mostly similar for the diamond-bearing gneisses and eclogite, but are significantly different in the low-grade schist (Fig. 13). In the diamond-grade gneisses, the inherited cores show a different pattern from those of the metamorphic overgrowths and display relatively high heavy REE (HREE) concentration and a flat REE pattern, whereas the diamond-bearing UHP domains are characterized by a steep pattern. The low-*P* mineral-bearing rims mostly show the same pattern as the UHP domains, but some have a negative Eu anomaly, suggesting overgrowth coexisting with plagioclase. Zircons from eclogite have no Eu anomaly and mostly have the same pattern as those of the diamond-grade UHP domains. In the low-grade schist, zircon shows a clearly different REE pattern, characterized by a higher abundance of light REE (LREE) and a significant negative Eu anomaly. The metamorphic overgrowth shows slightly higher HREE concentration than the inherited core. Because the inherited core has mostly remained in crystals, the large amount of zircon forming the overgrowth could not be derived from partial dissolution of crystals. The Zr may be derived from the decomposition of Zr-bearing phases such as biotite and ilmenite, or from intergranular fluids during metamorphism.

P–T–time history of the Kokchetav UHP–HP rocks

The ages obtained from SHRIMP analyses of different zircon domains suggest four discrete stages of the Kokchetav zircon growth: Middle Proterozoic for inherited cores, 537 ± 9 Ma for

Table 2. *Isotopic ages of the Kokchetav UHP–HP rocks*

Isotopic method	Protolith age (Ma)	UHP peak age (Ma)	Retrograde age (Ma)	Reference
U–Pb zircon assisted by inclusion	1300–1100	537 ± 9	507 ± 8	1
U–Pb zircon (average)	*c*. 2000	530 ± 7		2
Sm–Nd garnet and omphacite	*c*. 2200	533 ± 20		3
Pb–Pb whole rock	*c*. 1500			4
Ar–Ar muscovite			517 ± 5	4
Ar–Ar biotite			516 ± 5	4

References: 1, Katayama *et al*. (2001); 2, Claoue-Long *et al*. (1991); 3, Jagoutz *et al*. (1990); 4, Shatsky *et al*. (1999).

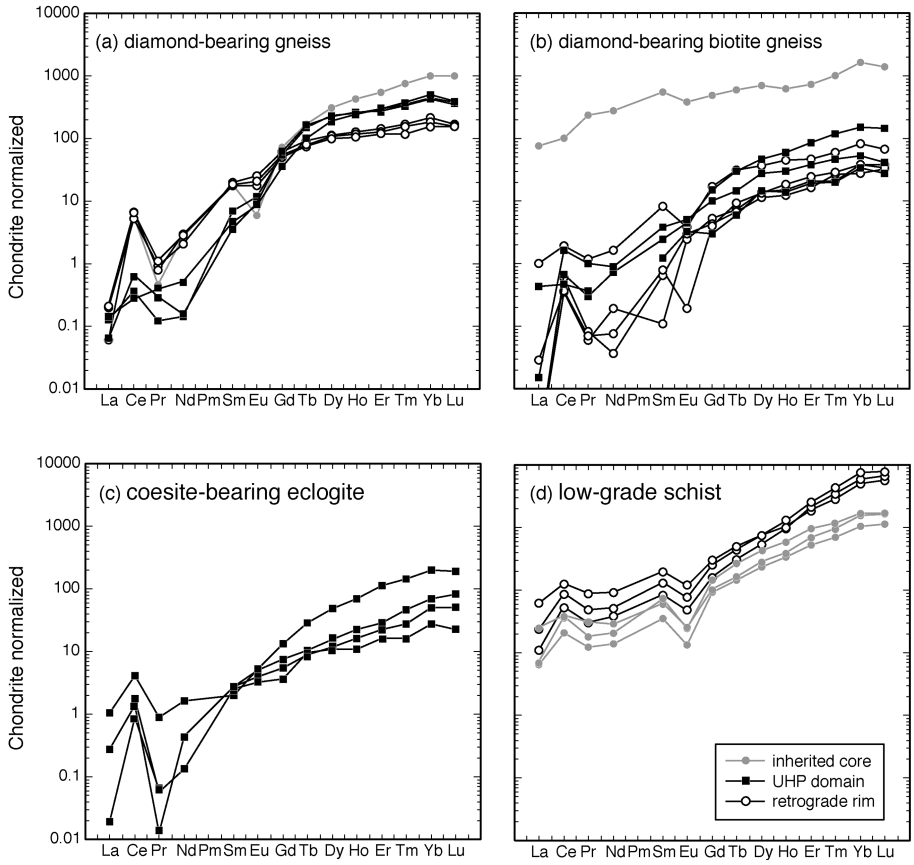

Fig. 13. REE patterns of zircon from diamond-bearing gneisses (**a**, **b**), eclogite (**c**), and low-grade schist (**d**). REE patterns are normalized to chondrite (Anders & Grevesse 1989).

cores, 507 ± 8 Ma for rims, and 456–461 Ma for outer rims (Fig. 14). The core and rim ages are weighted mean ages with 2σ errors calculated using Isoplot (Ludwig 1991), at a 95% confidence level.

An inherited zircon core of diamond-bearing gneiss yields a Middle Proterozoic age as an upper intercept age. The zircon core from low-grade schist yields a concordant age of 1280 ± 51 Ma, and oscillatory mantles yield 1138–1143 Ma. This indicates that the protolith of the Kokchetav UHP–HP rocks formed or was originally metamorphosed in the Middle Proterozoic. Claoue-Long *et al*. (1991) reported that zircon xenocrysts have concordant ages in the Early Proterozoic (*c*. 2000 Ma). The protolith of the Kokchetav UHP–HP rocks therefore contained various components of Proterozoic age.

The 537 Ma age of the diamond-bearing domains is clearly related to the UHP (peak) metamorphism. This age is slightly older than that of 530 ± 7 Ma reported by Claoue-Long *et al*. (1991). The discrepancy may be due to their calculation of the mean age involving various zircon domains including the UHP and later overprinting stages. Although the texture and distribution of inclusions suggest that some zircons have grown during prograde metamorphism (Katayama *et al*. 2000*a*), the averaging

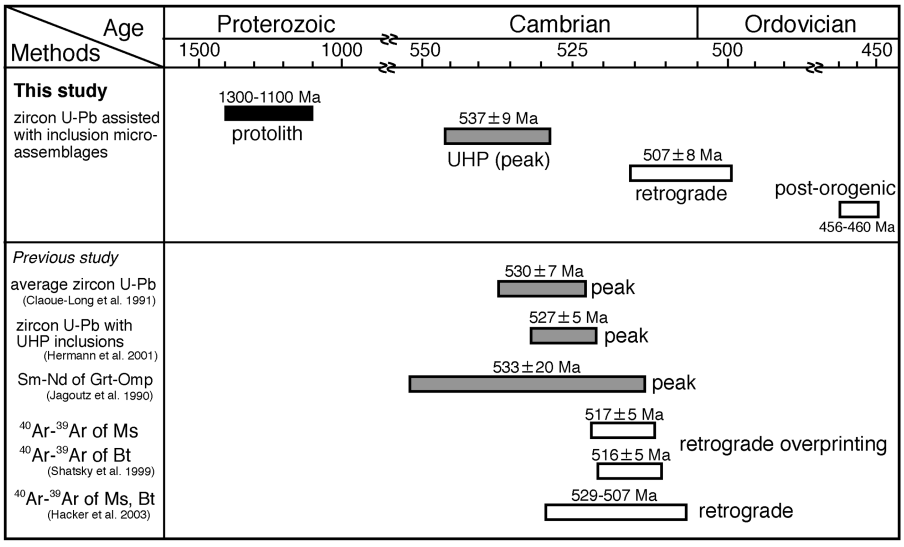

Fig. 14. Comparison of isotopic ages of this study and previous studies. The inclusion-assisted zircon U–Pb method provides the timing of the various stages. The peak zircon age of Claoue-Long *et al*. (1991) is considered as a mixed age of the different stages because of no identification of inclusions and internal zonal structure.

of the UHP zircon domains may have prevented clear differentiation between the ages of prograde and peak metamorphism. Hermann *et al*. (2001) also reported a U–Pb zircon age in this massif, but they show similar ages of distinct zircon domains and conclude a peak metamorphic age of 527 ± 5 Ma. Various *P–T* conditions of the Kokchetav UHP peak metamorphism have been estimated and are summarized in Table 3 and Figure 15. The minimum peak pressure of 40 kbar at 800 °C is constrained by the occurrence of microdiamonds. The high K_2O content in clinopyroxene (up to 1.0 wt%) from eclogite indicates a pressure >60 kbar (Okamoto *et al*. 2000). Ogasawara *et al*. (2000) noted that the occurrence of dolomite in diamond-bearing dolomite marble constrains the maximum pressure to >70 kbar. Peak temperatures have been estimated using the garnet–clinopyroxene geothermometer, which yields 880–910 °C (Zhang *et al*. 1997) from garnet–biotite gneiss, 950–1050 °C (Okamoto *et al*. 2000), 920–1000 °C (Shatsky *et al*. 1995) and 785 °C (Zhang *et al*. 1997) from eclogite, and 960 °C (Zhang *et al*. 1997) and 980 °C (Ogasawara *et al*. 2000) from diamond-bearing dolomitic marble. The garnet–biotite and garnet–phengite geothermometers yield temperatures ranging from 800 to 920 °C for garnet–biotite gneiss (Shatsky *et al*. 1995). In the eclogites, omphacite inclusions in zircon contain considerable amounts of Ca-Eskola component (up to 9.6 mol%). Based on the experimental calibration in mid-ocean ridge basalt (MORB) systems (e.g. Poli & Schmidt 1995), such high Ca-Eskola content requires 60–80 kbar as the peak-metamorphic condition. Clinopyroxene inclusions from the diamond-bearing gneisses contain much higher Ca-Eskola component (up to 18.6 mol%) than those of eclogites. However, experimental results for sediment compositions show a wide range of Ca-Eskola content depending on the starting composition and mineral assemblages (e.g. Domanik & Holloway 1996). The potassium solubility in clinopyroxene is sensitive to pressure and considered as a potential geobarometer when it coexists with the potassium-buffered minerals (e.g. Luth 1997; Okamoto *et al*. 2000). Diopside inclusions coexisting with diamond and phlogopite from the dolomitic marble (Fig. 5e) have a high K_2O content (up to 0.54 wt%), which requires pressures of *c*. 60–80 kbar based on the experimental results for the phlogopite–diopside system (Luth 1997). Zircon contains both garnet and clinopyroxene inclusions in the diamond-bearing domains. The Fe–Mg partitioning between garnet and clinopyroxene of Krogh (1988) yields peak temperatures of 920–1020 °C at a pressure of 60 kbar. The calculated temperatures are mostly consistent with previous estimates for the UHP rocks, but are slightly higher than those of the matrix phases. This may result from the strong retrogression of matrix phases, whereas the

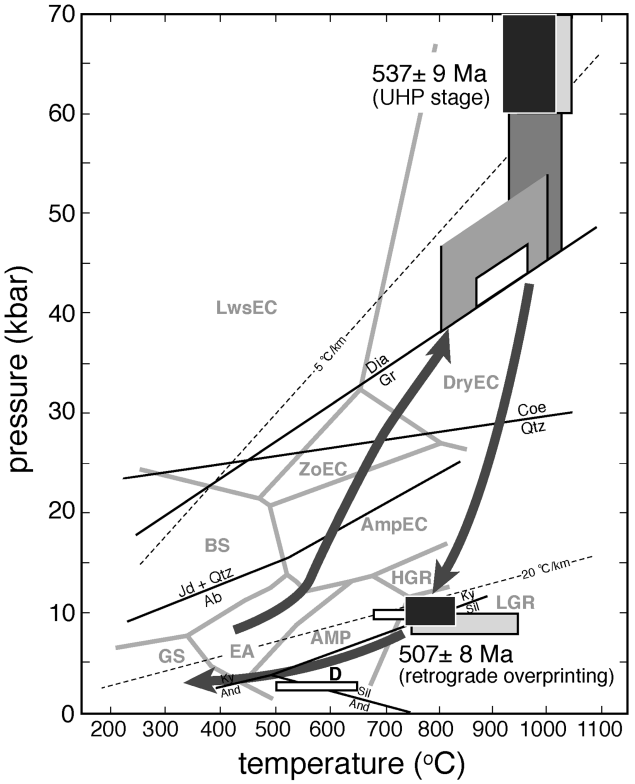

Fig. 15. Generalized *P–T*–time path for UHP–HP metamorphic rocks from the Kokchetav massif with geotherms of 5 °C km^{-1} and 20 °C km^{-1} (modified after Katayama *et al*. 2001). The *P–T* estimates are derived from this study (black field) and previous studies (Shatsky *et al*. 1995; Zhang *et al*. 1997; Ogasawara *et al*. 2000; Okamoto *et al*. 2000; Terabayashi *et al*. 2002). SHRIMP analysis of zircon domains differentiates the metamorphic history of the Kokchetav UHP–HP rocks into four stages: 1100–1400 Ma protolith age (stage 1); 537 ± 9 Ma for the UHP metamorphic origin (stage 2); 507 ± 8 Ma for the retrograde overprint origin (stage 3); 456–460 Ma for late granitoid intrusion origin (stage 4). Petrogenetic grids, subdivision of eclogite facies, stability fields of Al_2SiO_5 polymorphs, and reaction curves diamond = graphite, coesite = quartz and jadeite + quartz = albite are from Holdaway (1971), Bundy (1980), Holland (1980), Bohlen & Boettcher (1982) and Oh & Liou (1998). The box labelled D represents the *P–T* condition of Daulet Suite (Terabayashi *et al*. 2002). Abbreviations: GS, greenschist facies; EA, epidote-amphibolite facies; Am, amphibolite facies; LGR, low-pressure granulite facies; HGR, high-pressure granulite facies; BS, blueschist facies; AmpEC, amphibole-eclogite facies; ZoEC, zoisite-eclogite facies; LwsEC, lawsonite-eclogite facies; DryEC, dry eclogite facies.

Table 3. P–T *estimate of various rock types in the Kokchetav UHP rocks*

Rock type	Locality	Prograde stage	Peak stage	Retrograde stage	Reference
Eclogite	Kumdykol		970–1110 °C, 60–80 kbar	840 °C, <15 kbar	1
Grt–Bt gneiss	Kumdykol		950–1100 °C, >40 kbar	740–790 °C, *c*. 10 kbar	1
Dolomitic marble	Kumdykol	<850 °C, 28 kbar	980–1020 °C, 60–70 kbar		1
Eclogite	Kumdykol		840–1000 °C, >40 kbar		2
Eclogite	Kumdykol		785 °C, >30 kbar	680 °C, *c*. 10 kbar	3
Eclogite	Kumdykol		1000 °C, 60 kbar	750–950 °C, *c*. 10 kbar	5
Grt–Bt gneiss	Kumdykol		800–920 °C, >40 kbar		2
White schist	Kulet	430–580 °C, 8–19 kbar	750–800 °C, >28 kbar		3
Pyroxene–carbonate rock	Kumdykol		1120 °C, >40 kbar		2
Dolomitic marble	Kumdykol		900–1000 °C, >40 kbar	790 °C	3
Dolomitic marble	Kumdykol		980–1250 °C, 40–70 kbar	800–950 °C, 15 kbar	4

References: 1, this study; 2, Shatsky *et al*. (1995); 3, Zhang *et al*. (1997); 4, Ogasawara *et al*. (2000); 5, Okamoto *et al*. (2000).

inclusions in zircon have better preserved primary compositions of the UHP metamorphism.

The 507 Ma age of the outer rims corresponds to late-stage metamorphic overprinting, because these domains surround diamond- and coesite-bearing cores, and contain low-*P* mineral inclusions such as graphite, quartz, plagioclase and chlorite. Replacement of garnet by biotite, amphibole and/or plagioclase, and symplectite of plagioclase and amphibole after pyroxene in eclogite and pelitic gneiss, indicate that these rocks underwent amphibolite-facies retrogression (Shatsky *et al*. 1995; Zhang *et al*. 1997; Okamoto *et al*. 2000). Ar/Ar ages of secondary muscovite and biotite have been reported to be 517 ± 5 Ma (Shatsky *et al*. 1999). They are slightly older than those of zircon rims; however, the Ar/Ar age and our zircon rim U/Pb age are within uncertainty. The variation of rim ages (488–517 Ma; Fig. 12) may reflect continuous retrogression from amphibolite facies to greenschist facies during exhumation. Zhang *et al*. (1997) estimated retrograde temperatures of 680–790 °C from recrystallization of garnet–biotite in marble and amphibole–plagioclase in eclogite at amphibolite-facies conditions. Symplectic intergrowth of ilmenite, albite, augite and amphibole between omphacite and garnet from eclogite indicates pressures lower than 10 kbar and temperatures ranging from 750 to 950 °C (Zhang *et al*. 1997). In dolomitic marble, the highest $MgCO_3$ in Mg-calcite constrains the minimum *P*–*T* conditions higher than 25 kbar and 800 °C for the exhumation stage (Ogasawara *et al*. 2000). Zircon from the diamond-bearing gneiss contains chlorite inclusions of similar composition to those of matrix chlorite. Matrix garnets are replaced by chlorite, and the Fe–Mg partitioning geothermometer between garnet and chlorite (Grambling 1990) yields temperatures of 740–790 °C at pressure of 10 kbar (Fig. 15). In low-grade schist of the Daulet Suite, zircons show no age component around 537 Ma, and outer zircon rims yield ages of 461–516 Ma, which are similar to the retrograde ages of the diamond-bearing gneisses. The low-grade rocks have experienced maximum *P*–*T* conditions of *c*. 2.5 kbar and 500–650 °C (Terabayashi *et al*. 2002). Two outer rim domains yield apparently younger ages of 456–460 Ma (Fig. 12). They are interpreted to originate from late thermal events related to the large volume of granitoids intrusions in the Ordovician–Silurian (Dobretsov *et al*. 1995).

Tectonic implications

The chronological data including the inclusion-assisted zircon ages suggest the following tectonic synthesis for the Kokchetav UHP–HP massif. In the Late Proterozoic, an ocean existed between the Siberian craton and the Kokchetav microcontinent. Most of the Kokchetav metamorphic terrane consists of protoliths of a microcontinent rifted from the Siberian craton; bimodal volcanic rocks, shallow marine or terrestrial sediments and quartzo-feldspathic rocks in the UHP–HP belt support the rifting origin. The Sm–Nd model age indicates 2.2–2.3 Ga for the protolith, as do zircon xenocrysts of 1.2–2.0 Ga (Jagoutz *et al*. 1990; Claoue-Long *et al*. 1991; Katayama *et al*. 2001). Palaeogeographical reconstructions and the REE pattern of the metasediments in this massif support a passive margin origin (Mossakovsky & Dergunov 1985; Shatsky *et al*. 1999). The Proterozoic supracrustal rocks were then subducted with downgoing lithosphere to mantle depths during Middle Cambrian times (527–554 Ma). The UHP metamorphism took place at depths exceeding 150 km. Microdiamond and coesite crystallized, and were trapped in zircon at that time. The subducted supracrustal rocks returned to mid-crustal levels in the Late Cambrian. The thermal structure within the UHP–HP unit implies substantial differential movement, with more ductile, higher grade material being extruded from much greater depths, and being juxtaposed, in the nappe core, against progressively cooler rocks at shallower levels. The exhumed UHP rocks were juxtaposed against lower grade rocks of the Daulet Suite, which represents the footwall to the UHP–HP slab. The tectonic juxtaposition of the dehydrated UHP–HP rocks underlying the low-grade Daulet Suite rocks would allow infiltration of fluids and effectively obliterate the UHP–HP matrix mineral assemblages (Terabayashi *et al*. 2002). After the collisional event, widespread island-arc volcanism occurred, with subjacent, synkinematic and later anorogenic granitoid pluton intruding this massif during the Ordovician and Silurian.

Various mechanisms for exhumation of UHP metamorphic rocks from mantle depths have been proposed (e.g. Ernst 1971; Hacker & Peacock 1995; Maruyama *et al*. 1996). Taking the weighted mean ages of UHP metamorphism (537 Ma) and late amphibolite-facies overprinting (507 Ma), exhumation from diamond-grade depths (*c*. 60 kbar, 1000 °C) to mid-crustal depths (*c*. 10 kbar, 800 °C) must have been completed within about 30 Ma. This suggests that about 150 km of uplift must have occurred within about 30 Ma, leading to an average exhumation rate of 0.5 cm a^{-1}. However, this is a minimum rate because the mean ages of zircon cores and rims may include the prograde metamorphism and the later greenschist-facies overprinting, respectively. In previous studies, exhumation rates have been calculated systematically using several different isotopic methods and their combinations, including the Sm–Nd, U–Pb, Rb–Sr, and Ar–Ar systems. However, the zircon U–Pb method assisted with inclusion micro-assemblage and zonal structural image allows us to clarify the timing of the various stages of evolution of the UHP–HP rocks by a single isotopic method (Fig. 14). The exhumation rate estimated here lies within the range calculated by various methods (0.2–1.0 cm a^{-1}) for the Dora Maira massif of the western Alps (Gebauer *et al*. 1997), the Betic Cordilleras of northern Spain (Zeck & Whitehouse 1999), the central Rhodope zone of northern Greece (Liati & Gebauer 1999), and the Dabie Mountains of central China (Maruyama *et al*. 1998). Liu *et al*. (2006) also used the inclusion-assisted zircon chronology for samples from the Sulu CCSD drillhole and found an exhumation rate of 0.7 ± 0.2 cm a^{-1}, which is similar to the range for the Kokchetav UHP–HP rocks. Based on titanite SHRIMP dating with inclusion assemblages, Rubatto & Hermann (2001) proposed extremely fast exhumation rate (3.4 cm a^{-1}) in the Dora Maira massif; however, their pressure estimation has large uncertainty because titanite contains jadeite-rich clinopyroxene (up to 38 mol%) but no diagnostic UHP minerals.

Relatively rapid exhumation is considered to be one of the factors for preservation of UHP mineral assemblages and prograde zonation of garnet in whiteschist (Parkinson 2000), which would be obliterated by a long time span at high temperatures and pressures. The rapid exhumation rate suggests slab decoupling between continental and oceanic lithospheres, resulting in isostatic rebound of sialic material, as the most plausible driving force for uplift of the Kokchetav UHP metamorphic rocks from mantle depths. This is consistent with geological and petrological evidence in the Kokchetav massif: subhorizontal internal structural fabrics and metamorphic zonation, paired subhorizontal bounding structures juxtaposing the nappe against lower grade or unmetamorphosed rock (Kaneko *et al*. 2000), and the thermobaric structure with the highest-grade (UHP) rocks occupying a medial position within the nappe (Ota *et al*. 2000).

Conclusions

(1) UHP mineral inclusions, including diamond and coesite, were preserved in zircon from the Kokchetav UHP–HP massif, whereas evidence of UHP metamorphism was mostly obliterated in the matrix assemblages as a result of the extensive overprinting during exhumation. In addition to the UHP phases, relics of prograde texture including diamond crystallization consuming graphite are identified as inclusions in zircon. The preservation of primary UHP and prograde evidence in zircon is probably due to zircon being impervious to fluid infiltration and being capable of retaining minerals of each metamorphic stage.

(2) Mineral inclusions exhibit a slightly different chemical composition from the matrix minerals. Clinopyroxene inclusions from eclogite contain higher Ca-Eskola component, up to 9.6 mol%, than those of matrix, and the breakdown of this component causes quartz exsolution in the matrix clinopyroxenes. Mineral compositions of inclusions preserved in zircon can constrain the metamorphic P–T conditions, and indicate a peak stage of 60–80 kbar and 900–1100 °C, and about 10 kbar and 740–790 °C for the retrograde stage.

(3) SHRIMP U–Pb dating of zircons assisted by inclusion micro-assemblages indicates four discrete phases of the Kokchetav UHP metamorphic evolution: a protolith of Middle Proterozoic age, UHP metamorphism at 537 ± 9 Ma, a late-stage amphibolite-facies overprint at 507 ± 8 Ma, and post-orogenic thermal events at 456–461 Ma. Although previous geochronological studies used different isotopic systems to constrain the metamorphic evolution, zircon geochronology assisted by inclusion micro-assemblages provides the timing of each stage of the complex metamorphic history of the UHP–HP rocks.

We thank C. D. Parkinson, Y. Kaneko, T. Ota, S. Omori, K. Okamoto, Y. Ogasawara, J. G. Liou, R. Y. Zhang, K. Ye, F. Liu and M. Ohta for discussion and suggestions, and H. Tabata, K. Yamauchi, N. Abe, T. Iizuka, Y. Sano, K. Terada and Y. Tsutsumi for analytical assistance. A. Zayachikovsky is gratefully acknowledged for helping in the separation of a large number of zircons. This study was supported by the Japan Society for the Promotion of Science. We are grateful to the organizers of the 2007 International Eclogite Field Symposium for giving us the opportunity to review our progress in zircon studies, and also J.G. Liou and an anonymous reviewer for crucial comments.

References

Anders, W. & Grevesse, N. 1989. Abundances of the elements: Meteoritic and solar. *Geochimica et Cosmochimica Acta*, **53**, 197–214.

Austrheim, H. 1998. Influence of fluid and deformation on metamorphism of deep crust and consequences for the geodynamics of collision zones. *In:* Hacker, B.R. & Liou, J.G. (eds) *When Continents Collide: Geodynamics and Geochemistry of Ultrahigh-Pressure Rocks*. Kluwer, Dordrecht, 297–323.

Bohlen, S.R. & Boettcher, A.L. 1982. The quartz–coesite transformation: A pressure determination and effects of other components. *Journal of Geophysical Research*, **87**, 7073–7078.

Bundy, F.P. 1980. The *P*, *T* phase and reaction diagram for elemental carbon. *Journal of Geophysical Research*, **85**, 6930–6936.

Carswell, D.A., Brueckner, H.K., Cuthbert, S.J., Krogh, T.E., Mehta, K., O'Brien, P.J. & Tucker, R.D. 2001. Coesite preservation within zircons in the Hareidland eclogites and the timing of ultrahigh-pressure metamorphism in the Western Gneiss Region of Norway. *In:* Ogasawara, Y. (ed.) *Fluid/Slab/Mantle Interactions and Ultrahigh-*P *Minerals: UHPM Workshop (extended abstracts)*. Waseda University, Tokyo, 111–115.

Chopin, C. & Sobolev, N.V., 1995. Principal mineralogic indicators of UHP in crustal rocks. *In:* Coleman, R.G. & Wang, X. (eds) *Ultrahigh-pressure Metamorphism*. Cambridge University Press, Cambridge, 96–133.

Claoue-Long, J.C., Sobolev, N.V., Shatsky, V.S & Sobolev, A.V. 1991. Zircon response to diamond pressure metamorphism in the Kokchetav massif, USSR. *Geology*, **19**, 710–713.

Claoue-Long, J.C., Compston, W., Roberts, J. & Fanning, C.M. 1995. Two Carboniferous ages: A comparison of SHRIMP zircon dating with conventional zircon ages and $^{40}Ar/^{39}Ar$ analysis. *In:* Berggren, W.A., Kent, D.V., Swisher, C.C., Aubry, M.-P. & Hardenbol, J. (eds) *Geochronology, Time Scales and Global Stratigraphic Correlation*. Society for Economic Paleontologists and Mineralogists, Special Publications, **54**, 3–21.

Coleman, R.G. & Wang, X. 1995. Overview of the geology and tectonics of UHPM. *In:* Coleman, R.G. & Wang, X. (eds) *Ultrahigh-pressure Metamorphism*. Cambridge University Press, Cambridge, 1–28.

Dobretsov, N.L., Sobolev, N.V., Shatsky, V.S., Coleman, R.G. & Ernst, W.G. 1995. Geotectonic evolution of diamondiferous paragneisses, Kokchetav complex, northern Kazakhstan—the geologic enigma of ultra-high pressure crustal rocks within a Palaeozoic foldbelt. *Island Arc*, **4**, 267–279.

Domanik, K.J. & Holloway, J.R. 1996. The stability and composition of phengitic muscovite and associated phases from 5.5 to 11 GPa: Implications for deeply subducted sediments. *Geochimica et Cosmochimica Acta*, **60**, 4133–4150.

Eggins, S.M., Kinsley, L.P.J. & Shelley, J.M.G. 1998. Deposition and element fractionation processes during atmospheric pressure laser sampling for analysis by ICP-MS. *Applied Surface Science*, **127**, 278–286.

Ernst, W.G. 1971. Metamorphic zonations on presumably subducted lithospheric plates from Japan, California, and the Alps. *Contributions to Mineralogy and Petrology*, **34**, 45–59.

Gebauer, D., Schertl, H.P., Brix, M. & Schreyer, W. 1997. 35 Ma old ultrahigh-pressure metamorphism and evidence for very rapid exhumation in the Dora Maira Massif, Western Alps. *Lithos*, **41**, 5–24.

Grambling, J.A. 1990. Internally-consistent geobarometry and H_2O barometry in metamorphic rocks: the example garnet–chlorite–quartz. *Contributions to Mineralogy and Petrology*, **105**, 617–628.

Hacker, B.R. & Peacock, S.M. 1995. Creation, preservation and exhumation of coesite-bearing ultrahigh-pressure metamorphic rocks. *In:* Coleman, R.G. & Wang, X. (eds) *Ultrahigh-pressure Metamorphism*. Cambridge University Press, Cambridge, 159–181.

Harley, S.L. & Carswell, D.A. 1995. Ultradeep crustal metamorphism: A prospective view. *Journal of Geophysical Research*, **100**, 8367–8380.

Hermann, J., Rubatto, D., Korsakov, A. & Shatsky, V.S. 2001. Multiple zircon growth during fast exhumation of diamondiferous, deeply subducted continental crust (Kokchetav Massif, Kazakhstan). *Contributions to Mineralogy and Petrology*, **141**, 66–82.

Holdaway, M.J. 1971. Stability of andalusite and the aluminium silicate phase diagram. *American Journal of Science*, **271**, 97–131.

Holland, T.J.B. 1980. The reaction albite = jadeite + quartz determined experimentally in the range 600–1200 °C. *American Mineralogist*, **65**, 129–134.

Iizuka, T. & Hirata, T. 2004. Simultaneous determination of U–Pb age and REE abundances of zircons using ArF excimer laser ablation–ICPMS. *Geochemical Journal*, **38**, 229–241.

Jagoutz, E., Shatsky, V.S. & Sobolev, N.V. 1990. Sr–Nd–Pb isotopic study of ultrahigh *PT* rocks from Kokchetav massif. *EOS Transactions, American Geophysical Union*, **71**, 1707.

Kaneko, Y. Maruyama, S., Terabayashi, M., *et al.* 2000. Geology of the Kokchetav UHP–HP metamorphic belt, northern Kazakhstan. *Island Arc*, **9**, 264–283.

Kaneko, Y., Katayama, I., Yamamoto, H., *et al.* 2003. Timing of Himalayan ultrahigh-pressure metamorphism: sinking rate and subduction angle of the Indian continental crust beneath Asia. *Journal of Metamorphic Geology*, **21**, 589–599.

Katayama, I. & Nakashima, S. 2003. Hydroxyl in clinopyroxene from the deep subducted crust: Evidence for H_2O transport into the mantle. *American Mineralogist*, **88**, 229–234.

Katayama, I., Zayachkovsky, A. & Maruyama, S. 2000*a*. Progressive P–T records from zircon in Kokchetav UHP–HP rocks, northern Kazakhstan. *Island Arc*, **9**, 417–428.

Katayama, I., Parkinson, C.D., Okamoto, K., Nakajima, Y. & Maruyama, S. 2000*b*. Supersilicic clinopyroxene and silica exsolution in UHPM eclogite and pelitic gneiss from the Kokchetav massif, Kazakhstan. *American Mineralogist*, **85**, 1368–1374.

Katayama, I., Maruyama, S., Parkinson, C.D., Terada, K. & Sano, Y. 2001. Ion micro-probe U–Pb zircon geochronology of peak and retrograde stages of ultrahigh-pressure metamorphic rocks from the Kokchetav massif, northern Kazakhstan. *Earth and Planetary Science Letter*, **188**, 185–198.

Katayama, I., Nakashima, S. & Yurimoto, H. 2006. Water content in natural eclogite and its implication for water transport into the deep upper mantle. *Lithos*, **86**, 245–259.

Konzett, J., Frost, D.J., Proyer, A. & Ulmer, P. 2008. The Ca-Eskola component in eclogitic clinopyroxene as a function of pressure, temperature and bulk composition: an experimental study to 15 GPa with possible implications for the formation of oriented SiO_2-inclusions in omphacite. *Contributions to Mineralogy and Petrology*, **155**, 215–228.

Korsakov, A.V., Shatsky, V.S. & Sobolev, N.V. 1998. First occurrence of

coesite in eclogites from the Kokchetav massif, Northern Kazakhstan. *Russian Geology and Geophysics*, **34**, 40–50.

Krogh, E.J. 1988. The garnet–clinopyroxene Fe–Mg geothermometer: A reinvestigation of existing experimental data. *Contributions to Mineralogy and Petrology*, **99**, 44–48.

Liati, A. & Gebauer, D. 1999. Constraining the prograde and retrograde *P–T–t* path of Eocene HP rocks by SHRIMP dating of different zircon domains: inferred rates of heating, burial, cooling and exhumation for central Rhodope, northern Greece. *Contributions to Mineralogy and Petrology*, **135**, 340–354.

Liou, J.G., Zhang, R.Y. & Ernst, W.G. 1994. An introduction of ultrahigh-*P* metamorphism. *Island Arc*, **3**, 1–24.

Liou, J.G., Zhang, R.Y., Ernst, W.G., Rumble, D. & Maruyama, S. 1998. High-pressure minerals from deeply subducted metamorphic rocks. *In:* Hemley, R.J. (ed.) *Ultrahigh-pressure Mineralogy: Physics and Chemistry of the Earth's Deep Interior*. Mineralogical Society of America, Reviews in Mineralogy, **37**, 33–96.

Liu, F., Xua, Z.Q., Katayama, I., Yang, J., Maruyama, S. & Liou, J.G. 2001. Mineral inclusions in zircons of para- and orthogneiss from pre-pilot drillhole CCSD-PP1, Chinese Continental Scientific Drilling Project. *Lithos*, **59**, 199–215.

Liu, F., Xu, Z., Liou, J.G., Katayama, I., Masago, H., Maruyama, S. & Yang, J. 2002. Ultrahigh-*P* mineral inclusions in zircons from gneissic core samples of the Chinese Continental Scientific Drilling Site in eastern China. *European Journal of Mineralogy*, **14**, 499–512.

Liu, F., Liou, J.G. & Xue, H.M. 2006. Identification of UHP and non-UHP orthogneisses in the Sulu UHP terrane, eastern China: Evidence from SHRIMP U–Pb dating of mineral inclusion-bearing zircons. *International Geology Review*, **48**, 1067–1086.

Liu, J., Ye, K., Maruyama, S., Cong, B. & Fan, H. 2001. Mineral inclusions in zircon from gneisses in the ultrahigh-pressure zone of the Dabie Mountains, China. *Journal of Geology*, **109**, 523–535.

Ludwig, K.R. 1991. *Isoplot—a plotting and regression program for radiogenic isotope data*. US Geological Survey Open-File Report, **91-445**.

Luth, R.W. 1997. Experimental study of the system phlogopite–diopside from 3.5 to 17 GPa. *American Mineralogist*, **82**, 1198–1209.

Mao, H.K. 1971. The system jadeite ($NaAlSi_2O_6$)–anorthite ($CaAl_2Si_2O_8$) at high pressures. *Carnegie Institution of Washington, Yearbook*, **69**, 163–168.

Maruyama, S., Liou, J.G. & Terabayashi, M. 1996. Blueschists and eclogites of the world and their exhumation. *International Geology Review*, **38**, 485–594.

Maruyama, S., Tabata, H., Nutman, A.P., Morikawa, T. & Liou, J.G. 1998. SHRIMP U–Pb geochronology of ultrahigh-pressure metamorphic rocks of the Dabie Mountains, Central China. *Continental Dynamics*, **3**, 72–85.

Masago, H. 2000. Metamorphic petrology of the Barchi-Kol metabasites, western Kokchetav UHP–HP massif, northern Kazakhstan. *Island Arc*, **9**, 358–378.

Massonne, H.J. 2001. First find of coesite in the ultrahigh-pressure metamorphic region of the Central Erzgebirge, Germany. *European Journal of Mineralogy*, **13**, 565–570.

Mossakovsky, A.A. & Dergunov, A.V. 1985. The Caledonides of Kazakhstan, Siberia and Mongolia: a review of structure, development history and paleotectonic environments. *In:* Gee, D.G. & Sturt, B.A. (eds) *The Caledonide Orogen—Scandinavia and Related Areas*. Wiley, New York, 1201–1215.

Ogasawara, Y., Ohta, M., Fukasawa, K., Katayama, I. & Maruyama, S. 2000. Diamond-bearing and diamond-free metacarbonate rocks from Kumdy-Kol in the Kokchetav Massif, northern Kazakhstan. *Island Arc*, **9**, 400–416.

Ogasawara, Y., Fukasawa, K. & Maruyama, S. 2002. Coesite exsolution from titanite in UHP marble from the Kokchetav Massif. *American Mineralogist*, **87**, 452–461.

Oh, C.W. & Liou, J.G. 1998. A petrogenetic grid for eclogite and related facies under high-pressure metamorphism. *Island Arc*, **7**, 36–51.

Okamoto, K., Liou, J.G. & Ogasawara, Y. 2000. Petrological study of the diamond grade eclogite in the Kokchetav massif, northern Kazakhstan. *Island Arc*, **9**, 379–399.

Okamoto, K., Katayama, I., Maruyama, S. & Liou, J.G. 2006. Zircon-inclusion mineralogy of a diamond-grade eclogite from the Kokchetav massif, northern Kazakhstan. *International Geology Review*, **48**, 882–891.

Ota, T., Terabayashi, M., Parkinson, C.D. & Masago, H. 2000. Thermobaric structure of the Kokchetav UHP–HP massif deduced from a north–south traverse in the Kulet and Saldat-kol regions, northern Kazakhstan. *Island Arc*, **9**, 328–357.

Parkinson, C.D. 2000. Coesite inclusions and prograde compositional zonation of garnets in whiteschists of the Kokchetav Massif, Kazakhstan: a record of progressive UHP metamorphism. *Lithos*, **52**, 215–233.

Parkinson, C.D. & Katayama, I. 1999. Metamorphic microdiamond and coesite from Sulawesi, Indonesia: evidence of deep subduction as SE Sundaland Margin. *EOS Transactions, American Geophysical Union*, F1181.

Parkinson, C.D., Motoki, A., Onishi, C.T. & Maruyama, S. 2001. Ultrahigh-pressure pyrope–kyanite granulites and associated eclogites in NeoProterozoic nappes of southeast Brazil. *In:* Ogasawara, Y. (ed.) *Fluid/Slab/Mantle Interactions and Ultrahigh-*P *Minerals: UHPM Workshop (extended abstracts)*. Waseda University, Tokyo, 87–90.

Poli, S. & Schmidt, M.W. 1995. H_2O transport and release in subduction zones: Experimental constraints on basaltic and andesitic systems. *Journal of Geophysical Research*, **100**, 22299–22314.

Rubatto, D. & Hermann, J. 2001. Exhumation as fast as subduction? *Geology*, **29**, 3–6.

Rubatto, D., Gebauer, D. & Compagnoni, R. 1999. Dating of eclogite-facies zircons: the age of Alpine metamorphism in the Sesia–Lanzo Zone (Western Alps). *Earth and Planetary Science Letters*, **167**, 141–158.

Rubie, D.C. 1986. The catalysis of mineral reactions by water and restrictions on the presence of aqueous fluid during metamorphism. *Mineralogical Magazine*, **50**, 399.

Sano, Y., Hidaka, H., Terada, K., Shimizu, H. & Suzuki, M. 2000. Ion microprobe U–Pb zircon geochronology of the Hida gneiss: Finding of the oldest minerals in Japan. *Geochemical Journal*, **34**, 135–153.

Schertl, H.P. & Schreyer, W. 1996. Mineral inclusions in heavy minerals of the ultrahigh-pressure metamorphic rocks of the Dora–Maira massif and their bearing on the relative timing of the petrological events. *In:* Basu, A. & Hart, S. (eds) *Earth Processes: Reading the Isotopic Code*. American Geophysical Union, Geophysical Monograph, **95**, 331–342.

Shatsky, V.S., Sobolev, N.V. & Vavilov, M.A. 1995. Diamond-bearing metamorphic rocks of the Kokchetav massif, northern Kazakhstan. *In:* Coleman, R.G. & Wang, X. (eds) *Ultrahigh Pressure Metamorphism*. Cambridge University Press, Cambridge, 427–455.

Shatsky, V.S., Jagoutz, E., Sobolev, N.V., Kozmenko, O.A., Parkhomento, V.S. & Troesch, M. 1999. Geochemistry and age of ultra-high pressure rocks from the Kokchetav massif, northern Kazakhstan. *Contributions to Mineralogy and Petrology*, **137**, 185–205.

Smyth, J.R. 1980. Cation vacancies and the crystal chemistry of breakdown reactions in kimberlitic omphacites. *American Mineralogist*, **65**, 1185–1191.

Sobolev, N.V. & Shatsky, V.S. 1990. Diamond inclusions in garnets from metamorphic rocks. *Nature*, **343**, 742–746.

Song, S., Yang, J., Katayama, I., Liu, F. & Maruyama, S. 2001. Zircons and their inclusions from various rocks in the Dulan UHP metamorphic terrane, the north Qaidam, NW China. *In:* Ogasawaka, Y. (ed.) *Fluid/Slab/Mantle Interactions and Ultrahigh-*P *Minerals: UHPM Workshop (extended abstracts)*. Waseda University, Tokyo, 116–120.

Stacey, J.S. & Kramers, J.D. 1975. Approximation of terrestrial lead isotope evolution by a two-stage model. *Earth and Planetary Science Letters*, **26**, 207–221.

Tabata, H., Yamauchi, K., Maruyama, S. & Liou, J.G. 1998. Tracing the extent of a UHP metamorphic terrane: Mineral-inclusion study of zircons in gneisses from the Dabie Shan. *In:* Hacker, B.R. & Liou, J.G. (eds) *When Continents Collide: Geodynamics and Geochemistry of Ultrahigh-Pressure Rocks*. Kluwer, Dordrecht, 261–273.

Terabayashi, M., Ota, T., Yamamoto, H. & Kaneko, Y. 2002. Contact metamorphism of the Daulet Suite by solid intrusion of the Kokchetav HP–UHPM slab. *In:* Parkinson, C.D., Katayama, I., Liou, J.G. & Maruyama, S. (eds) *The Diamond-Bearing Kokchetav Massif, Kazakhstan*. Universal Academy Press, Tokyo, 413–426.

Ye, K., Yao, Y., Katayama, I., Cong, B., Wang, Q. & Maruyama, S. 2000. Large areal extent of ultrahigh-pressure metamorphism in the Sulu ultrahigh-pressure terrane of East China: new implications from coesite and omphacite inclusions in zircon of granitic gneiss. *Lithos*, **52**, 157–164.

Zeck, H.P. & Whitehouse, M.J. 1999. Hercynian, Pan-African, Proterozoic and Archean ion-microprobe zircon ages for a Betic–Rif core complex, Alpine belt, W Mediterranean—consequences for its *P–T–t* path. *Contributions to Mineralogy and Petrology*, **134**, 134–149.

Zhang, R.Y., Liou, J.G., Coleman, R.G., Ernst, W.G., Sobolev, N.V. & Shatsky, V.S. 1997. Metamorphic evolution of diamond-bearing and associated rocks from the Kokchetav massif, northern Kazakhstan. *Journal of Metamorphic Geology*, **15**, 479–496.

Received 22 February 2008; revised typescript accepted 4 February 2009.
Scientific editing by Simon Cuthbert and David Peate.